

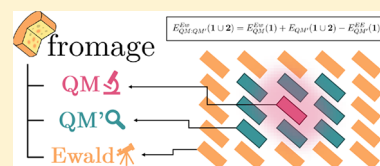
ONIOM(QM:QM') Electrostatic Embedding Schemes for Photochemistry in Molecular Crystals

Miguel Rivera,¹ Michael Dommett,¹ and Rachel Crespo-Otero*¹

School of Biological and Chemical Sciences, Queen Mary University of London, Mile End Road, London E1 4NS, U.K.

S Supporting Information

ABSTRACT: Understanding photoinduced processes in molecular crystals is central to the design of highly emissive materials such as organic lasers and organic light-emitting diodes. The modeling of such processes is, however, hindered by the lack of excited state methodologies tailored for these systems. Embedding approaches based on the Ewald sum can be used in conjunction with excited state electronic structure methods to model the localized excitations which characterize these materials. In this article, we describe the implementation of a two-level ONIOM(QM:QM') point charge embedding approach based on the Ewald method, the ONIOM Ewald embedded cluster (OEEC) model. An alternative self-consistent method is also considered to simulate the response of the environment to the excitation. Two molecular crystals with opposing photochemical behavior were used to benchmark the results with single reference and multireference methods. We observed that the inclusion of an explicit ground state cluster surrounding the QM region was imperative for the exploration of the excited state potential energy surfaces. Using OEEC, accurate absorption and emission energies as well as S_1 – S_0 conical intersections were obtained for both crystals. We discuss the implications of the use of these embedding schemes considering the degree of localization of the excitation. The methods discussed herein are implemented in an open source platform (fromage, <https://github.com/Crespo-Otero-group/fromage>) which acts as an interface between popular electronic structure codes (Gaussian, Turbomole, and Molcas).



1. INTRODUCTION

Highly emissive organic crystals have great potential for the development of optoelectronic and photonic devices such as organic light-emitting diodes and organic lasers.^{1–3} The electronic structure of the constituent monomers, intermolecular interactions, and the electrostatic field in the crystal environment all contribute to the competition between radiative and nonradiative pathways, such as internal conversion and intersystem crossing. The exploration of excited state potential energy surfaces (PESSs) in the solid state can help decipher the role of these interconnected factors and rationalize observed quantum yields.

Excitations in molecular crystals are normally localized over a few molecular units and can be strongly influenced by the periodic crystal environment.⁴ This poses a challenge for traditional electronic structure methods, which have been designed to describe either highly localized or periodic delocalized electronic states. In this context, embedding techniques represent a viable option by combining higher quantum mechanical levels of theory to describe the excited region (QM) and more approximate methods for the crystal environment (QM' or molecular mechanics (MM)).⁵

Within the ONIOM scheme, the QM' method can be chosen to be plane-wave density functional theory (DFT)^{6,7} for a natural description of the lattice periodicity, although this usually means sacrificing the electrostatic embedding. Correlated wave-function-in-DFT periodic embedding approaches are a promising alternative.^{8–10} One of the most common approaches is to use cluster models to describe the periodic

crystal.^{11–13} The cluster is extracted from the atomic lattice positions and provides an energetic description of the short-range interactions with the QM region.

In the case of ionic or highly polar crystals, long-range interactions can be of great importance since the electrostatic potential is slowly and conditionally convergent.¹⁴ The long-range Coulomb interactions with distant atomic centers are therefore traditionally evaluated using Ewald summation techniques.^{15–17} The expression for the Ewald potential at position r is

$$V^{\text{Ewald}}(\mathbf{r}) = \sum_{L_s} q_s \frac{\text{erfc}(\gamma|\mathbf{r} - \mathbf{L} - \mathbf{R}_s|)}{|\mathbf{r} - \mathbf{L} - \mathbf{R}_s|} + \frac{4\pi}{v_c} \sum_{\mathbf{G} \neq 0} \frac{1}{G^2} e^{-G^2/4\gamma^2} \left[\sum_s q_s e^{i\mathbf{G}(\mathbf{r} - \mathbf{R}_s)} \right] \quad (1)$$

where \mathbf{L} and \mathbf{G} are the real and reciprocal space lattice translations, q_s are the charges of each site s of the unit cell at positions \mathbf{R}_s , γ is the Ewald constant, and v_c is the volume of the unit cell. Here, the direct sum electrostatic potential has been recast as a sum of two rapidly converging series. Short-range Coulomb terms are calculated in direct space, and long-range interactions are calculated using a Fourier series in reciprocal space. To evaluate the Ewald potential on a lattice site r_i , the self-potential of the charge must be subtracted to avoid a singularity

Received: November 21, 2018

Published: March 13, 2019

which amounts to replacing the $L = 0$ and $s = i$ case of the first term of eq 1 with $-\frac{2/7q_i}{\sqrt{\pi}}$.^{14,18–20}

When considering embedded finite cluster models, the electrostatic embedding can be modified to reflect the Ewald potential. In this case, the electrostatic interactions affecting the QM region extend beyond just the short range and up to the infinitely large in a periodic system. Klintonberg et al. developed a methodology where a large array of point charges is fitted to reproduce the exact Ewald potential inside the QM region of a cluster model.^{15,21,22} This procedure has been used for the investigation of ionic crystals and the calculation of NMR parameters in organic crystals.^{15,23,24} Sokol et al. have implemented a related method in Chemshell to model defects in ionic materials.^{25,26} An alternative is the procedure proposed by Abarenkov and Sushko, where compensating point charges are added within unit cells to approach the Ewald potential.^{27,28}

Ewald embedding methods have been used with QM:MM and ONIOM approaches allowing the evaluation of the short-range non-Coulombic interactions.^{29–34} However, a simpler variant is the point charge embedding approach (PCE) where only the Coulomb interactions are considered, using point charges, and nonelectrostatic interactions are neglected.^{5,15} The performance of these methods for the investigation of excited state PESs of molecular crystals is relatively unexplored. Recently, Ciofini and co-workers^{35–37} implemented an Ewald PCE scheme based on the method proposed by Derenzo et al.²² In order to consider mutual polarization effects of the crystal environment, a self-consistent algorithm was employed in the investigation of a crystal displaying aggregation-induced emission.³⁶ Self consistent procedures are typical tools used in QM:MM schemes when the polarization of the environment is important.^{38–40}

Herein we present the implementation of Ewald embedding approaches for the description of PESs of molecular crystals, with specific focus on the treatment of excited state minima and conical intersections. We show that, due to the lack of short-range non-Coulombic interactions, geometry optimization with the PCE method can be extremely problematic. As a solution, we implement an Ewald-embedded QM:QM' cluster model that can be used to explore the PESs of flexible molecules. We assess the efficacy of these schemes with two crystals based on 2'-hydroxychalcone (HC1 and HC2, shown in Figure 1). These molecules undergo excited state intramolecular proton transfer (ESIPT), where the large changes in electronic structure in the excited state pose a challenge to embedding methods.

We have previously investigated HC1 and HC2 in the context of aggregation induced emission (AIE).^{41,42} The population of

the keto (K^*) and enol (E^*) excited states depends on the identity of the substituents and crystal packing.⁴² HC1 displays emission in the crystal with promising properties to be used in solid state lasers⁴³ and predominantly forms herringbone-type aggregates. In contrast, HC2's decay is mainly nonradiative and its crystal structure features mainly π -stack dimers. Their PESs were found to be particularly sensitive to the electrostatic environment. The AIE character of HC1 can be understood using the restricted access to conical intersections (RACI) model^{44,45} wherein upon aggregation the energy of the S_1-S_0 conical intersections increases, thereby blocking nonradiative deactivation pathways and enhancing the emissive response.

The paper is organized as followed. First, we present the different embedding models and the details of their implementation. Next, we describe how to choose the size of the high-level QM region, an important step in the division of the cluster regions. We then determine the effect of different point charge embedding schemes and assess their overall performance. In our conclusions, we suggest a protocol for researchers studying excited states in molecular crystals. The presented methodologies are implemented in a new open-source platform: fromage (FRameworkOrk for Molecular AGgregate Excitations).

2. EMBEDDING SCHEMES

We consider two electrostatic Ewald embedding approaches to investigate excited states in molecular crystals: PCE and a two-level ONIOM(QM:QM') model. For the PCE approach, where only the Coulombic interactions are considered, we adopt a strategy similar to that proposed by Wilbraham et al.³⁵ The atomic charges were obtained using the Ewald program from Derenzo et al.²² after being modified to allow noninteger charge values. The effect of the polarization of the environment was considered for both methods within a self-consistent embedding algorithm. These approaches were implemented in fromage; the source code and the documentation are available online.^{46,47}

In the Ewald program,²² an array of about 10^4 charges is generated from a supercell. Three zones are defined; the central region (zone I) is where the highest level of theory will be used. It is spherically surrounded by a buffer region (zone II) of approximately 500 point charges. Charges of both zone I and zone II are held constant. The rest of the charges (zone III) are altered to reproduce the Ewald potential in the central and buffer regions. The algorithm removes any artificial dipole moment introduced in the procedure. A detailed description of the method and the corresponding program can be found in ref 22.

The implementation of PCE in fromage consists of electronic structure calculations at zone I atomic sites, embedded in the atomic charges of zones II and III. For clarity, we refer to zone II and III charges as Ewald charges. Excited state energies are obtained with time-dependent DFT (TDDFT), CASSCF, CASPT2, and CC2 via interfaces with Gaussian,⁴⁸ Molcas,⁴⁹ and Turbomole.⁵⁰ An interface with DFTB+⁵¹ is under development. The atomic charges can be obtained from molecular or periodic crystal calculations. We consider restrained electrostatic potential (RESP), Mulliken, and natural bond order (NBO) from molecular calculations and RESP, Mulliken, Hirshfeld, and atoms-in-molecules (AIM) charges from periodic calculations. Currently, atomic charges can be read from Gaussian and CP2K.

fromage provides tools for the exploration of PESs of molecular crystals. The L-BFGS minimization algorithm is used to locate stationary points. A complete characterization of

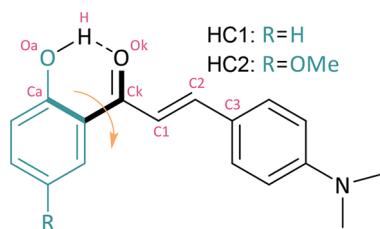


Figure 1. Molecular diagram of 2'-hydroxychalcone derivatives HC1 and HC2. The access to conical intersections for these molecules is centered around the rotation of the blue group about the dihedral angle shown in bold. The notable atoms with large partial charge are labeled in pink.

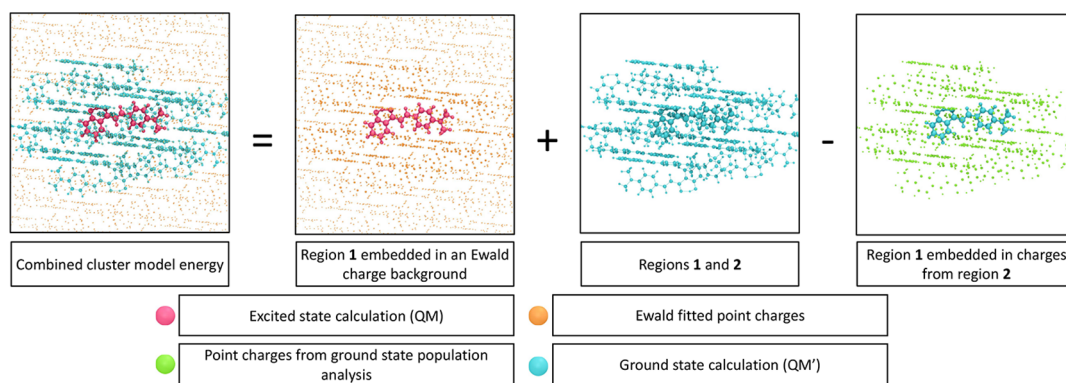


Figure 2. Visual representation of the main energy equation for the Ewald embedded cluster model.

excited state potential energy surfaces in molecular crystals requires the description of conical intersections. We have implemented the penalty function method of Levine et al.⁵² to optimize minimal energy conical intersection (MECI) geometries. In contrast with other methods,⁵³ this approach does not require nonadiabatic coupling vectors. A function of the averaged S_1 and S_0 energies (\bar{E}_{1-0}) and the S_1 – S_0 energy gap (ΔE) is minimized:

$$F = \bar{E}_{1-0} + \sigma \frac{\Delta E^2}{|\Delta E| + \alpha} \quad (2)$$

where σ is a Lagrangian multiplier and α is a parameter such that $\alpha \ll |\Delta E|$. This algorithm is implemented in frotage for CASSCF, CC2, and TDDFT electronic methods. We would like to emphasize that even when multireference quantum methods are preferable for modelling S_1 – S_0 crossings,^{54,55} in many cases single-reference methods such as TDDFT can provide a qualitative description of these regions of the PES.⁵⁵ Non-adiabatic dynamics simulations with these methods have shown for multiple systems that methods such as ADC(2) and CC2 can provide reasonable results.^{56,57} In the case of TDDFT, a careful selection of the functional is required.^{58,59} Considering the computational cost of multireference methods and the sensitivity of their active space, it can at times be necessary to resort to single-reference methods. However, their performance near S_1 – S_0 crossings should be carefully tested by comparison with multireference calculations.

Geometry optimization and conical intersection search become problematic within the PCE scheme because of the lack of short-range non-Coulombic interactions which results in overpolarization effects (see section 4.2). To overcome these limitations, we formulate an ONIOM⁶⁰ Ewald embedded cluster (OEEC) model. It is devised as an extension of the commonly used ONIOM embedded cluster model (OEC) which usually only includes electrostatic embedding up to the range of the cluster. We consider a QM:QM' scheme rather than QM:MM to avoid the need for specific parametrization.

A graphical representation of our EEC model is shown in Figure 2. The EEC model is comprised of two regions: the central region 1 (corresponding to zone I in the Ewald program) and nearest-neighbor molecules (2). Region 2 should be large enough to include the most important short-range non-electrostatic interactions with the QM cluster. The buffer region defined for Ewald (zone II) does not necessarily correspond to region 2.

Identically to those with PCE, excited state calculations of region 1 are embedded in Ewald charges and are performed at

the highest level of theory—with a QM method—yielding the energy $E_{\text{QM}}^{\text{Ew}}(1)$. Two ground state energy calculations are further performed at a QM' level of theory: the energies of the cluster composed of regions 1 and 2 ($E_{\text{QM}'}(1 \cup 2)$) and the energy of region 1 electrostatically embedded in the charges of 2 ($E_{\text{QM}'}^{\text{EE}}(1)$). The total energy in the cluster is calculated as follows:

$$E_{\text{QM:QM}'}^{\text{Ew}}(1 \cup 2) = E_{\text{QM}}^{\text{Ew}}(1) + E_{\text{QM}'}(1 \cup 2) - E_{\text{QM}'}^{\text{EE}}(1) \quad (3)$$

The hybrid gradients are defined accordingly.

In the OEEC scheme, Coulombic interactions of any distance between region 1 and the crystal are described at the higher level of theory (QM). For excited state calculations, this represents the interaction between an excited central region and the environment in the ground state, unless particular charges are considered in the Ewald algorithm (vide infra). In contrast, the short-range non-Coulombic interactions between 1 and 2 are considered at the QM' ground state level, which recovers some of the short-range contributions and improves the description provided by PCE. Since non-Coulombic interactions are considered in the ground state, for fixed geometries the energy gaps are equivalent to those obtained with the PCE. The selection of the QM' level of theory depends on the available computational resources. Previous studies on truncated cluster models have shown that low levels of theory such as HF/STO-3G achieve accurate results.^{6,12,35,36,61}

The choice of charges in the embedding of $E_{\text{QM}'}^{\text{EE}}(1)$ in eq 3 should provide an approximate cancellation of the Coulombic interactions between regions 1 and 2 in the ground state (see the Supporting Information).⁶² We therefore use charges obtained from a QM' population analysis in the embedding of $E_{\text{QM}'}^{\text{EE}}(1)$, while using charges from a QM ground state calculation in the embedding of $E_{\text{QM}}^{\text{Ew}}(1)$ for an accurate representation of the lattice electrostatic potential. In contrast, traditional ONIOM schemes use the same partial charge values for both embeddings. This is done in order to mitigate overpolarization effects stemming from the use of point charges; these effects are particularly severe when the inter-region boundary crosses a bond and link atoms need to be used. However, in the cases discussed herein, the region boundary is defined inter- rather than intramolecularly and most intermolecular contacts are larger than 4 Å, which allows us to select charges of the highest quality in the embedding of $E_{\text{QM}}^{\text{Ew}}(1)$. This situation can be generalized to any organic molecular crystal with similar or higher sparsity in packing. Further extensions of these methods

Table 1. Embedding Models Used in This Study

acronym	full name	description
PCE	point charge embedding	point charge embedding fitted to match the Ewald potential
SC-PCE- S_1	self-consistent point charge embedding S_1	PCE computed self-consistently in S_1
SC-PCE- S_0	self-consistent point charge embedding S_0	PCE computed self-consistently in S_0
OEC	ONIOM embedded cluster	QM:QM' ONIOM cluster model with the QM region embedded in charges from the QM' region
OEEC	ONIOM Ewald embedded cluster	OEC with the QM region embedded in charges from PCE
SC-OEEC- S_1	self-consistent ONIOM Ewald embedded cluster S_1	OEC with the QM region embedded in charges from SC-PCE- S_1
SC-OEEC- S_0	self-consistent ONIOM Ewald embedded cluster S_0	OEC with the QM region embedded in charges from SC-PCE- S_0

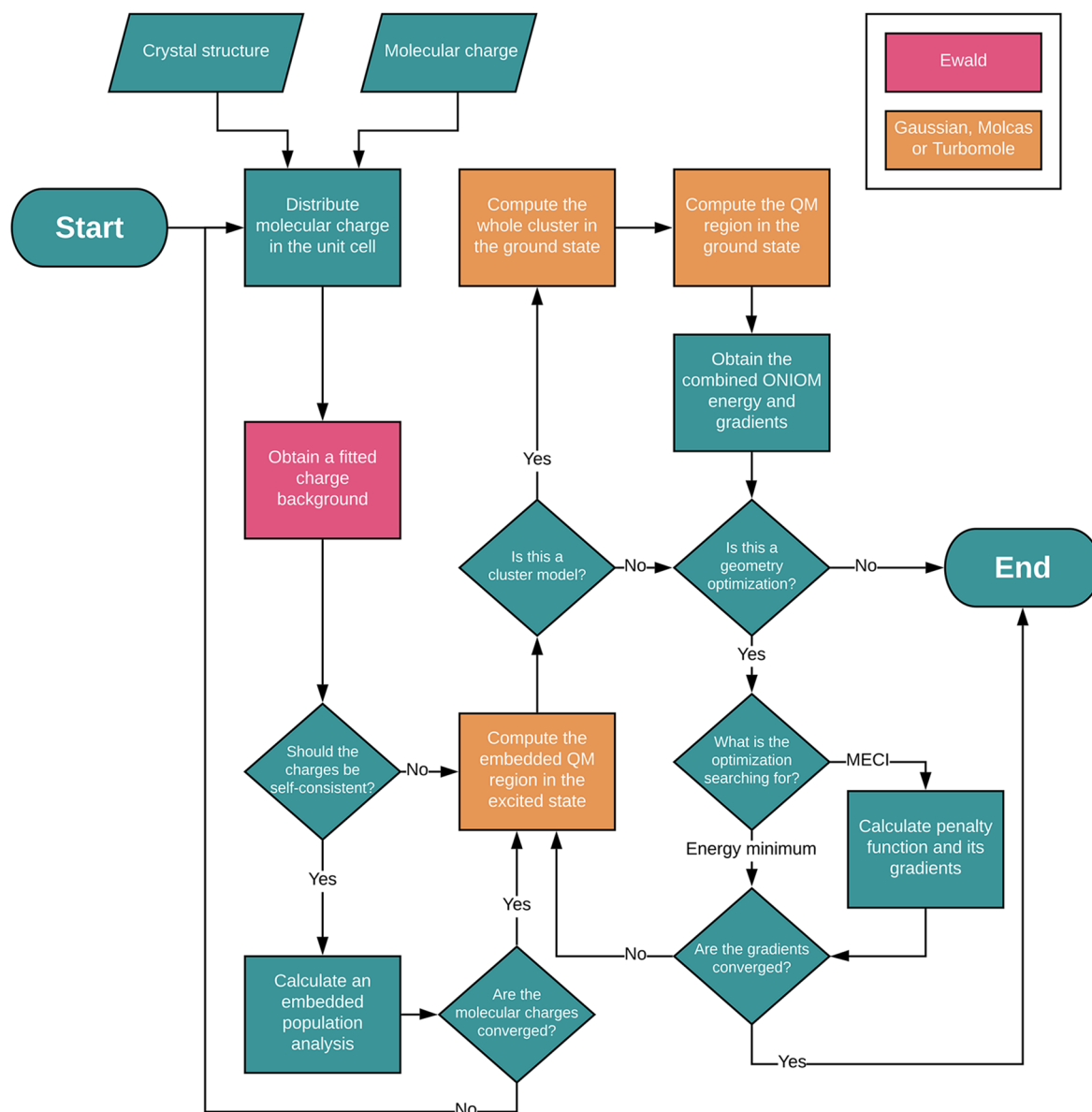


Figure 3. Flowchart of a calculation using the ONIOM Ewald embedded cluster (OEEC) and self-consistent ONIOM Ewald embedded cluster (SC-OEEC) models. The electronic program can be chosen by the user.

can be implemented to reduce artificial polarization⁶³ and make the methods useful for more dense systems. We are already working on this direction.

The alternative scheme where Ewald charges are used for the QM' calculations should provide a worse compensation of the

inter-region Coulombic interactions. For testing purposes, we have also implemented this scheme in fromage ($E_{QM'}^{Ew}(1)$ as the final term of eq 3). Nevertheless, the results obtained with this embedding scheme are similar to those obtained with the cluster charges for HCl, possibly due to a cancellation of errors. The

absorption energies are only deviated by 0.01 eV from those obtained with the original scheme. In the case of the emission energies from the K form, the value obtained with this version of OEEC is 2.24 eV which is in relative good agreement with the results obtained with other schemes (Table 3).

In order to consider the response of the environment to the excitation and recover mutual polarization effects, we employ the extension of self-consistent Ewald embedding to excited states proposed by Wilbraham et al.³⁵ Mutually polarizing embedding methods have been applied to a number of ground state systems.^{15,24,64,65} In the self-consistent approach, a QM-level calculation is carried out on a quantum cluster. A population analysis is then applied and the charge values are reassigned to the equivalent positions in the crystal. Those charges are then fitted using Ewald and another QM calculation is carried out. The loop between Ewald fitting and population analysis is repeated until convergence of the atomic charges. The new charge background is used for the electrostatic embedding of 1. In fromage, the self-consistent approach is implemented for the PCE and the QM/QM' approaches (SC-PCE and SC-OEEC). We consider two versions which may represent different physical situations in the crystal (discussed in section 4.1). The first, SC-PCE-S₁, closely corresponds to the embedding proposed by Wilbraham et al.; it uses excited state charges as an initial charge background and iterates with excited state population analyses. The second, SC-PCE-S₀, has a ground state initial charge background and performs ground state population analyses. We extend these terms to SC-EEC-S₁ and SC-EEC-S₀. For ease of reading, the embedding models are listed in Table 1.

For SC-PCE-S₁, the convergence can be sped up by starting the loop from a ground state population analysis embedded in ground state Ewald charges. The final background was found to be very similar, with a root-mean-square deviation (RMSD) of $10^{-5} e^-$ for atomic charges. Another alternative is to perform the loop on a molecule which has already been optimized in the excited state using OEEC. In this case, the equilibration of the charge background is made to match the excited state minimum; however, this implies assigning charges from an excited state minimum configuration to region 2 molecules which are in their ground state minimum geometry.

Figure 3 describes the structure of fromage. The charge background can be chosen to be computed self-consistently, and the geometry optimization can be set to search for ground and excited state minima or MECI. Currently, region 2 is fixed in place during geometry optimization, although full cluster relaxation⁵³ is under development. For SC-OEEC, to recover point charges of the highest quality, the molecule of interest in the unit cell is first relaxed with OEEC. Furthermore, the self-consistent charge background is computed only for the first step, at the ground state OEEC geometry, in order to maintain a consistent PES throughout the relaxation.

3. COMPUTATIONAL DETAILS

The crystal structures of HC1 and HC2 were optimized using PBE-D2 as implemented in Quantum Espresso.⁶⁶ The plane-wave cutoff was 30 Ry, and the *k*-point meshes were $2 \times 3 \times 2$ and $2 \times 2 \times 1$ respectively, in accordance with the shapes of the unit cells. Subsequently, a single point PBE-D2/DZVP calculation was carried out using CP2K⁶⁷ to extract RESP, Hirshfeld, and Mulliken periodic charges. For AIM charges, an external program developed by Henkelman et al. was used to process the Quantum Espresso DFT charge density.^{68–71}

Molecular RESP charges were first calculated at the HF/3-21G(p) level for comparison with our previous ONIOM (QM:AMBER) calculations.⁴¹ Every other molecular population analysis (NBO, Mulliken, RESP for OEEC and SC-OEEC models) used ω B97X-D/6-311++G(d,p) as implemented in Gaussian.

For the seven charge schemes, 1000 checkpoints were sampled in the quantum cluster and 500 points had their values fixed to create a buffer region. The total charge background was comprised of 64 unit cells for HC1 and 32 for HC2. These numbers were chosen so as to create a sufficient amount of point charges²²—at least 10 000—while keeping an isotropic distribution in accordance with the shape and size of each unit cell.

Both molecular crystals were then investigated using a hierarchy of models. First, PCE was used with all of the charge types described above on a single QM-level monomer. When possible, the excited state geometries were optimized with TD- ω B97X-D/6-311++G(d,p). Next, the cluster models were introduced, using RESP charges from ω B97X-D/6-311++G(d,p) in the embedding of $E_{QM}^{EW}(1)$. OEC, OEEC, and SC-OEEC were all employed on a single monomer of the crystal embedded in a cluster of 21 molecules for HC1 and 16 molecules for HC2. The excited state minima and S₁–S₀ MECI were found using fromage. For the location of S₁–S₀ MECI, the parameters in eq 2 were initially set to 0.02 hartree for α and 3.5 for σ . σ was then increased if the gap was found to be insufficiently small after optimization of *F*.

For the comparison of different points along the potential energy surface, we use a fixed charge background. This avoids varying classical energy contributions due to charge–charge interactions and different Ewald constants.¹⁴ In this article, we used the charge background obtained for the FC conformation, although for crystals with significant Frenkel exciton occurrences, S₁ self-consistent charges could provide a better description of the excited states. All backgrounds are available in fromage, leaving the choice up to the user.

Overall, the QM methods employed were TD- ω B97X-D/6-311++G(d,p) using Gaussian, RI-CC2/TZVP, and RI-CC2/SV(P) using Turbomole and SA-2-CASSCF(12,11)/6-31G(d) and MS-2-CASPT2(12,11)/6-31G(d) using Molcas, all with PCE, OEEC, and SC-OEEC. The QM' method was HF/STO-3G using Gaussian, and the low level embedding charges of $E_{QM}^{EE}(1)$ were accordingly chosen to be from RESP calculations at the same level of theory. For the self-consistent population analysis procedure, a convergence criterion of 0.001 e⁻ for the mean deviation of charge values between subsequent steps was chosen. Where necessary, under-relaxation was employed with a damping factor of 0.75 to address convergence issues in the self-consistent loop such as divergence or oscillation. For excited state self-consistent backgrounds, using initial charges from an isolated excited state molecule or a Ewald embedded ground state molecule yielded the same final background although the latter method converged in fewer steps.

For comparison, single monomers were also optimized in the ground and excited states using TD- ω B97X-D/6-311++G(d,p) in a vacuum and using polarizable continuum models (PCMs) and self-consistent PCM (SC-PCM) with a dichloromethane (DCM) solvent as implemented in Gaussian. Exciton couplings were computed using the diabaticization scheme proposed by Aragó and Troisi, which considers short and long-range contributions.⁴

4. RESULTS

4.1. Localization of the Excitation: Size of the QM Region. The use of embedding techniques for excited state calculations in molecular crystals presumes the localization of the excitation over a few molecular units. However, the degree of localization is often unclear and unpredictable, conflicting with the intrinsic truncation of a cluster model. Therein lies the necessity for different kinds of embedding techniques which represent different physical situations. Before comparing the effect of these techniques, we wish to clarify how they relate to exciton localization in our model systems.

In the case of OECC, the Ewald charges arise from a ground state population analysis. Consequently, this approach represents a localized excitation in region 1 before the environment has responded to the change in electronic density. To instead represent the extreme situation where all molecules are excited simultaneously and are mutually responsive, charges from excited state calculations can be used. We call this scheme SC-OEEC- S_1 (or, in general, SC-OEEC- S_n). If the molecules in the QM' region are considered to be in the ground state and the S_0 charges are self-consistently updated, an alternative SC-OEEC- S_0 scheme can be defined. It is expected that the SC-OEEC- S_1 scheme will perform better in systems where excitation is highly delocalized and the S_1 electron density is significantly different from the ground state. We have implemented all these schemes in fromage so that the user can select the most suitable scheme for the system under investigation. The degree of localization of the excitation in a molecular crystal will depend on the exciton coupling with neighboring molecules and the experimental conditions for absorption.

In order to investigate the excitonic features of the excited state electron densities of the HC1 and HC2 crystals, we consider a tetramer (Figure 4) embedded in ground state Ewald

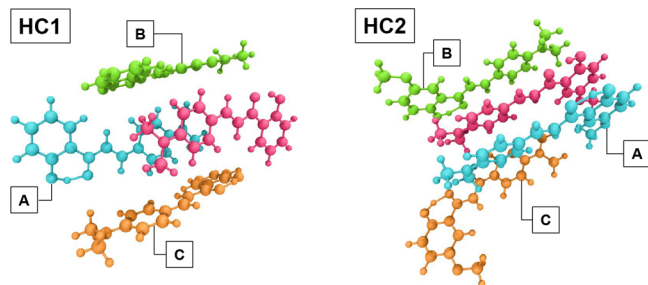


Figure 4. Selected tetramer configurations from both crystals. The molecule in pink is optimized using OECC.

charges as a reference. This model includes the short-range Coulomb interactions between the central and three surrounding molecules explicitly and thus should provide a benchmark to evaluate the ability of the different embedding schemes to describe the excited states considering a smaller QM region. Note that, in contrast to the monomer, where the bright state is S_1 , for the tetramer the bright states are S_4 and S_5 for HC1 and HC2, respectively.

Figure 5 shows the S_n-S_0 density differences obtained for the bright state at Franck–Condon geometry (FC) and the K^* S_1 excited state minimum geometries. The plots for the first five excited states can be found in the Supporting Information. An important degree of localization is observed on monomers and dimers for both crystals, despite four molecules being included in the QM region. Consequently, we expect that, with

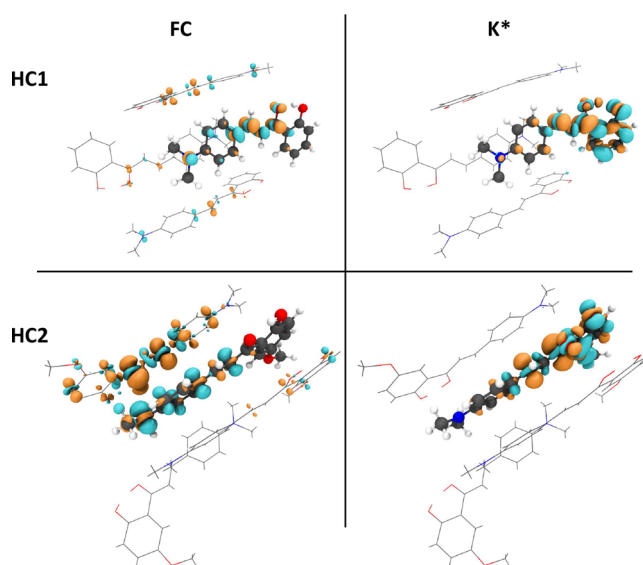


Figure 5. S_n-S_0 density differences obtained at TD- ω B97X-D/6-311++G(d,p) level of theory for the tetramer model (excited state density is shown in orange, ground state in blue). For the FC geometries, the tetramer's bright states were considered ($n = 4$ for HC1 and $n = 5$ for HC2); for K^* , $n = 1$. All configurations were obtained by optimizing the geometry of the central molecule with OECC.

embedding charges of sufficient quality, a QM region of one or two molecules would obtain accurate excited state energies.

Excitations are more localized in HC1 than in HC2, which correlates with the larger exciton couplings obtained for the latter. In the case of HC1, only the coupling with molecule B is larger than 0.1 eV (Supporting Information). For both crystals, in the K^* minimum, the excitation is clearly localized in the central molecule, which suggests that schemes such as OECC and SC-OEEC- S_0 could be best suited to describe this kind of situations (see discussion in sections 4.2 and 4.3). Additionally, the QM region with only one monomer should be able to describe emission from the K^* form, which is confirmed by the evolution of the energies with the size of the region (see section 4.3).

4.2. Point Charge Embedding: Electrostatic Effects in the Crystal. In this section, we analyze the performance of the PCE model and the effect of using different charges for the description of excited states in the HC1 crystal. Our analysis is based on the results obtained with a monomer in the QM region.

The experimental absorption in the solid state shows two bands which have previously been attributed to absorption from the E and K forms.^{43,72} Our calculations show that neither the crystal composed of K molecules nor the one with K surrounded by E molecules is stable in the solid state. Additionally, the experimental crystal structure does not seem to be consistent with a significant population of the K form in the ground state.⁷² Taking this into account, the presence of K in the ground state seems to be associated with dynamic processes activated in the experimental conditions. For example, at room temperature, large amplitude motions of the proton along the H-bonded bridge can reduce the S_1-S_0 energy gap to 2.76 eV, considering vibrational broadening. Additionally, given the ultrafast nature of the proton transfer in the solid state (3 ps⁷²), fast absorption from K forms generated in the excited state could also be possible. The dynamic nature of these processes is in line with the broad structure of the low energy band. Our focus is the

Table 2. Absorption, Emission, and K-MECI Energies (in eV) of HCl Embedded in Different Types of Ewald Point Charge Arrays^a

method	charge		absorption FC(E)	emission		S ₁ –S ₀ K-MECI
	type	basis		E*	K*	
		Molecular				
TD- ω B97X-D/6-311++G(d,p)	NBO	6-311++G(d,p)	3.28	3.10	2.67	4.35
	RESP	6-311++G(d,p)	3.30	3.12	2.66	4.41
	RESP (SC-PCE-S ₁)	6-311++G(d,p)	3.09	2.96	2.65	4.72
	RESP ^b	6-311++G(d,p)	3.37	-	2.69	4.37
	Mulliken	6-311++G(d,p)	1.56	1.51	1.47	4.42
	Mulliken	3-21G(d)	3.29	3.11	2.70	4.76
	Mulliken	6-31G(d)	3.35	3.16	2.70	4.68
RI-CC2/SV(P)	RESP	6-311++G(d,p)	3.11	2.95	2.35	3.82
RI-CC2/TZVP	RESP	6-311++G(d,p)	2.98	2.82	2.29	3.56
		Crystal				
TD- ω B97X-D/6-311++G(d,p)	RESP	DZVP	3.33	3.15	2.68	4.32
	AIM	DZVP	3.35	3.16	2.68	4.30
	Hirshfeld	DZVP	3.43	3.23	2.68	4.56
	Hirshfeld ^b	DZVP	3.50	3.20	2.28	2.89
	Mulliken	DZVP	2.95	2.85	2.64	4.20
TD- ω B97X-D/6-311++G(d,p)	no charges	–	3.52	3.31	2.67	4.76
	vacuum ^c	–	3.65	3.28	0.36	2.84
experimental ^{43,72}	–	–	2.9, 3.3	–	1.7–1.9	–

^aUnless specified the geometries were obtained at the ONIOM(TD- ω B97X-D/6-311++G(d,p):AMBER) level of theory. K-MECI energies are relative to the ground state energy of the Franck–Condon (FC) minimum.⁴² ^bOptimized geometries within the PCE environment. ^cGeometry optimized in a vacuum.

analysis of the higher energy band which corresponds to the absorption in the E form.

To estimate the effect of vibrational broadening on the position of the absorption maximum, we use the nuclear ensemble method⁷³ as implemented in Newton-X⁷⁴ with TD- ω B97X-D/6-311++G(d,p) embedded in RESP charges. The position of the E absorption maximum (3.21 eV, 0.1 eV shift with respect to the vertical excitation with the same method) is in excellent agreement with the experimental value (Supporting Information).

To directly evaluate the effect of charges of different origin, we compare absorption, emission (from E* and K* forms), and S₁–S₀ MECI energies with Ewald embedding. Given that the MECI associated with the enol pathway was consistently found to be at least 4 eV higher in energy than its keto counterpart, we will focus on the K-MECI deactivation pathway. The results are summarized in Table 2. In order to directly compare the impact of different charge partition schemes, we use the same geometry throughout, obtained at the ONIOM(TD- ω B97X-D/6-311++G(d,p):AMBER) level of theory.⁴²

Excited state calculations with PCE using non-Mulliken charges predict the maximum of absorption with close agreement to the experimental value of 3.3 eV. Overall, the effect of the embedding is to shift absorption to the red with respect to the energy obtained in a vacuum (3.65 eV). For calculations at fixed geometries, there is no significant dependence on whether the charges are obtained from molecular or crystal calculations. In particular, the energies obtained using RESP charges are consistent between the molecular and the crystal descriptions. In the context of the molecular organic crystals, this is not surprising as RESP charges are designed to match the electrostatic potential and crystal packing has but a small effect on the electronic structure of these molecules.

In contrast, calculations using Mulliken charges strongly depend on the choice of basis set (both the size and the type). With these charges, results with smaller basis sets are closer to the experimental value. They provide reasonable energies with 3-21G(p) and 6-31G(d), but fail to reproduce sensible values if a larger basis set is used (6-311++G(d,p)). This is in line with the well-known sensitivity of the Mulliken method to the basis set.

The experimental emission in the solid state has been attributed to the K* form.⁴² Regardless of the higher stability of K* in the excited state, emission from the E* form is expected to be close to the initial absorption and consequently reabsorbed. Accordingly, our TDDFT calculations predict emission from E* in the range 3.1–3.3 eV. Interestingly, emission from the K* form (~2.7 eV) is significantly deviated from the experimental values (1.7–1.9 eV).^{43,72} This is not improved by using self-consistent point charges in the SC-PCE-S₁ method, which is to be expected due to the localization of the excited state to one molecule (Figure 5). When the emission is calculated using RI-CC2, the energy is improved but is still deviated by more than 0.5 eV from the experiments.

The most significant factor is the geometry itself, obtained at QM:MM level. We show later that a better emission energy is obtained when optimization is done using the OEEC and SC-OEEC methods. When it comes to the optimization of excited state minima and S₁–S₀ MECI, the PCE approach was unsuccessful for most charge types, due to the lack of non-Coulombic short-range interactions and ensuing overpolarization effects. Only Hirshfeld and, in certain cases, crystal RESP charges were overall small enough in magnitude to allow for the determination of local minima. As such, optimization with PCE in general is not recommended for systems with a high degree of conformational flexibility.

As for S₁–S₀ MECI energies, all TDDFT results for the QM:MM geometries are more than 1 eV above the FC bright state energy (Table 2). The conical intersections are thus

rendered inaccessible as expected since HC1 displays aggregation-induced emission. The energies obtained with RI-CC2 are in the range 0.6–0.7 eV above their corresponding excitation energies, which also makes them inaccessible. These results are consistent within the RACI model but are overestimated with respect to the value of 3.97 eV obtained with QM:MM with a dimer in the QM region.⁴²

In the case of RESP charges, optimization within the PCE model does not significantly change the energetics previously evaluated with single point calculations. Indeed the structures are close to those reported at the QM:MM level of theory. The resulting relative energies are shown in Figure 6. For Hirshfeld charges, the effect of optimization is more significant reducing the K^* emission energies to 2.28 eV and making the S_1 – S_0 MECI accessible.

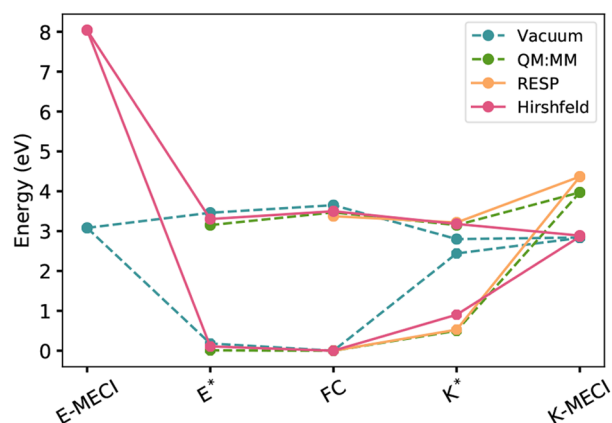


Figure 6. Energies HC1 in a vacuum and embedded in RESP and crystal Hirshfeld Ewald charges at different geometries. QM:MM energies were taken from ref 42.

Comparing the calculations in PCE and a vacuum at the same geometry highlights the main effects of the crystal electrostatic environment in the excited state. The excited states are overall stabilized, which reduces both the vertical excitation and conical intersection energies. However, the accessibility of the latter depends on the former, netting no clear difference in emissive behavior. A more substantial relative stabilization of the MECI is observable when the molecule is fully optimized in a vacuum. It reaches a highly distorted geometry which would be inaccessible in the solid due to short-range interactions of the closely packed neighboring molecules.

Our simulations show some of the drawbacks of the PCE method, in particular for its use in geometry optimization. Because of the effects of overpolarization and the lack of short-range non-Coulombic interactions, electrostatic forces can become too large and some nuclear configurations become unstable. Consequently, we do not recommend the use of PCE for geometry optimizations. While the method is effective in some cases,^{75,76} it is unpredictable whether it will provide reliable geometries for all regions of the PES. To mitigate these problems, we implemented a two-level embedded cluster model.

4.3. Embedded Cluster Models: Potential Energy Surfaces in the Crystal. We obtained the geometries of notable regions of the PES for HC1 and HC2 crystals using the OEEC and its self-consistent variant SC-OEEC methods. Table 3 shows the absorption and emission energies obtained after optimization of FC and K^* forms using these models.

Table 3. Absorption and Emission Energies for Both Model Systems after Geometry Optimization with Cluster Models^a

cluster model	HC1		HC2	
	FC	K^*	FC	K^*
OEEC	3.37	2.06	3.41	2.07
SC-OEEC- S_1	3.08	2.60 (2.12) ^b	3.34	2.15
SC-OEEC- S_0	3.27	2.19	3.40	2.07
OEC	3.27	2.40	3.42	2.03
PCM	3.32	2.36	3.72	2.44
SC-PCM	3.00	2.66	3.01	2.21
ONIOM QM:MM (monomer) ⁴²	3.32	2.72	3.50	2.17
ONIOM QM:MM (dimer) ⁴²	3.27	2.61	3.29	2.19
experimental ^{43,72}	2.9, 3.3	1.7–1.9	–	1.8

^aThe level of theory was TD- ω B97X-D/6-311++G(d,p). Energies are in eV. ^bCharges obtained for the K^* form in S_1 .

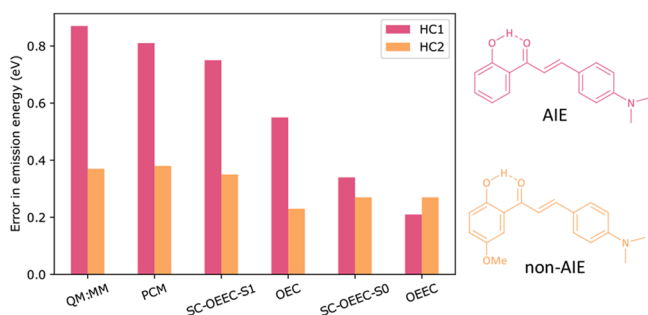
Geometry optimization using the embedded cluster method produces ground state geometries very similar to those from QM:MM; consequently the absorption energies are not significantly altered between PCE and OEEC or SC-PCE- S_1 and SC-OEEC- S_1 provided that RESP charges are used throughout (Table 2). For comparison, we have added the results obtained with ONIOM (QM:MM) including one and two molecules in the QM region and with the OEC model. Moreover, we present results in PCM and its self-consistent variant, both in DCM solvent, since continuum models are a common method employed to reflect the electrostatic environment in molecular condensed matter.⁷⁷

For all cluster models, the effect of the polarized response of the environment is to reduce the vertical excitation. This is also observed in the comparison between the PCM and SC-PCM models and when the size of the QM region increases from a molecule to dimer. The results obtained with the SC-OEEC procedure depend on the level of excitation in the self-consistent loop. If ground state charges are used, as expected, the energies are similar to those obtained with OEEC (3.27 and 3.37 eV for HC1 and 3.40 and 3.41 eV for HC2). The emission energies obtained with different methods strongly depend on the rotation angle (Figure 1). In a vacuum, the excited state minima show a significant deviation from their ground state planar structures. In the solid state, the K^* geometries obtained with QM:MM and SC-OEEC- S_1 are more planar (HC1, 6 and 9°; HC2, 16 and 12°, respectively, for the angle depicted in Figure 1) than those obtained with OEEC (HC1, 32°; HC2, 18°).

The optimization of the K^* form with the EEC model significantly improves the emission energies with respect to those obtained using QM:MM geometries. Scheme 1 summarizes the deviation of the calculated emission energies with respect to the experimental data.

For HC1, the result is 2.06 eV (TD- ω B97X-D/6-311++G(d,p)), which is in close agreement with the experimental value. As with the PCE method, the self-consistent background based on the excited state charges at the FC state does not improve the results (2.6 eV). If ground state E charges are employed in the self-consistent loop, the emission energies remain in better agreement with the experimental values. Indeed, given the level of localization of the excitation in these systems (Figure 5), the use of ground state charges seems to be more appropriate (SC-OEEC- S_0) with emission energy of 2.19 eV. An alternate version of SC-OEEC- S_1 is also employed where the self-consistent loop is carried out on a molecule in its OEEC

Scheme 1. Deviation with Respect to Experimental Values of Emission Energies of HC1 and HC2 Predicted by Different Embedding Models^a



^aReference experimental values were 1.8 eV for both HC1 and HC2 crystals.

optimized K^* geometry, which brings the emission energy to 2.12 eV. However, this charge background represents the situation where all molecules in the crystal exhibit charges from the keto form, which is highly unlikely since this would not represent a low energy excited state.

Comparison of the OEEC with the OEC model indicates that long-range interactions account for more than 0.3 eV in the K^* emission energy of HC1. Interestingly, while the energies for HC1 strongly depend on the charge background, the values for HC2 are less affected. In the case of HC2, SC-OEEC, OEEC, and OEC all provide very similar results (2.15, 2.07, and 2.07 eV), suggesting that the most important Coulomb effects are recovered at the short range. This is linked to the difference between the ground and excited state charges of these molecules. For HC1, excitation significantly alters the charges of carbon atoms in the bridge (Supporting Information). In the case of HC2 only the charge of the carbonyl carbon (C_k) changes more than $0.1 e^-$ upon excitation. Consequently, the S_1-S_0 energy gaps for HC1 are far more dependent on the electrostatic environment. Indeed improving the description of the short-range intermolecular interactions does not significantly alter the energy gaps, as illustrated by the behavior of the absorption and emission energies with the size of the QM region (see end of section). For both, HC1 and HC2, the emission from K^* is fairly well reproduced with only one molecule in the QM region, which is in line with the localized nature of the K^* (Figure 5).

Conical intersections play a key role in photophenomena, providing a radiationless decay funnel for the excited state. One of the features implemented in fromage is the searching of crossing geometries using the penalty function method of Levine et al.⁵² The molecules considered here can deactivate to the ground state in solution via conical intersections associated with intramolecular rotation.^{41,42} We optimize the S_1-S_0 MECI with the SA-2-CASSCF(12,11)/6-31G(d) and TD- ω B97X-D/6-311++G(d,p) methods within the OEEC scheme (Figure 7). For these systems, the geometries obtained with both levels of theory are in very good agreement.

In the crystal, the lowest energy conical intersection combines intramolecular rotation and a significant pyramidalization of the carbonyl carbon.⁴² In the gas phase, the lowest energy conical intersection only involves intramolecular rotation while the one also involving pyramidalization is higher in energy. Therefore one of the effects of the crystal environment is to modify the stability of the lowest energy conical intersections, which is

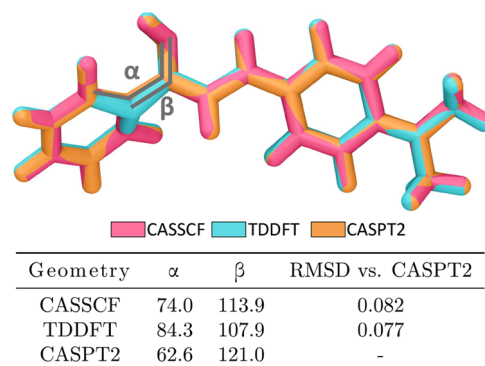


Figure 7. MECI geometries found with SA-2-CASSCF(12,11)/6-31G(d) and TD- ω B97X-D/6-311++G(d,p). Additionally, we include the configuration with least S_1-S_0 gap when scanning the β angle from the TDDFT geometry at MS-2-CASPT2(12,11)/6-31G(d) level. It is labeled CASPT2.

consistent with the results obtained with QM:MM calculations. This confirms that the effect of short-range interaction is essential in determining the geometry while the long-range interactions modulate the total energy. However, the net effect of the embedding on the total energies is highly system dependent.

Figure 8 shows the PES obtained with multireference methods. The vertical excitation obtained with SA-2-CASSCF(12,11)/6-31G(d) is significantly deviated from the experimental value (4.25 eV compared to 3.3 eV). Including dynamic electron correlation with MS-2-CASPT2(12,11)/6-31G(d) shifted the value to the red, in much better agreement with the experimental value (3.53 eV). The energy gap at the CASSCF conical intersection is too large with PT2 (1.02 eV), but using TDDFT geometries as reference can significantly narrow the gap. These are common challenges found in multireference calculations and are not due to the embedding approach.^{78–80} In order to further narrow the S_1-S_0 gap, the aromatic C was systematically displaced via the β angle (Figure 7). Figure 9 shows how this scan locates a conical intersection at an energy 0.8 eV above the FC energy. These examples show that the Ewald embedding methods can provide all the information required to fully characterize the PES in molecular crystals. All of these methods are available in fromage.

Given that the Ewald embedding methods describe the effect of the electrostatics of the whole crystal, they represent unique schemes to analyze the convergence of properties with the size of the QM region. Exploring these effects is essential in systems with significant excitonic effects. We consider the behavior of the energies and the accessibility of the S_1-S_0 MECI with the size of the QM region (Figure 10). We employ the TD- ω B97X-D/6-31G(d) level of theory, which provides a good description of different regions of the PES. For HC1, the energies of the bright state for FC and of the emission from K^* converge relatively quickly. On the other hand, the energy of the S_1-S_0 MECI increases with the size of the QM region for HC1 and decreases for HC2 respectively becoming less and more accessible. This is in line with the experimental behavior of both crystals.

5. CONCLUSION

In this paper, we analyze the behavior of different Ewald embedding schemes for the description of excited states in molecular crystals. With focus on the exploration of potential energy surfaces, we have implemented these methods in the

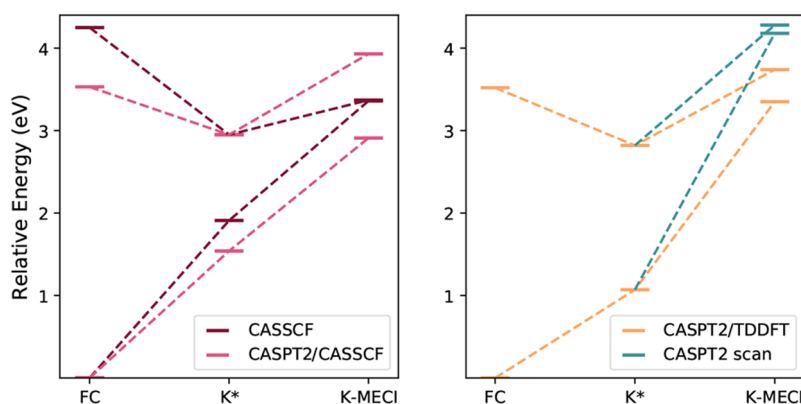


Figure 8. Relative energy diagrams showing the emission energy and accessibility of the MECI with multireference methods at the geometries shown in Figure 7. To minimize the CASPT2 S_1-S_0 gap at MECI configurations, a geometry scan was carried out as described in Figure 9. The newly optimized geometry is labeled “CASPT2 scan” and has a gap of 0.10 eV.

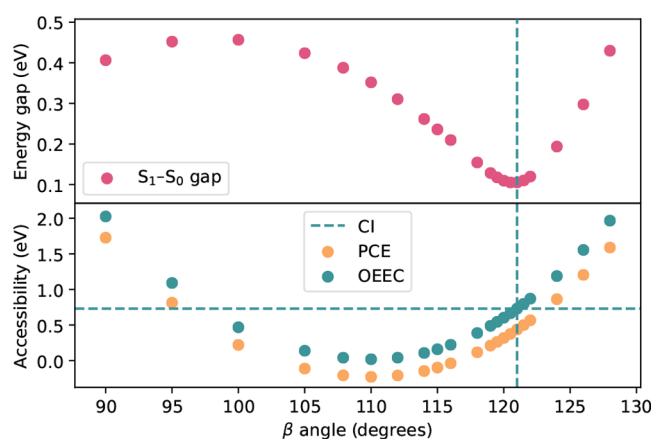


Figure 9. Plot of the S_1-S_0 gap, and the MECI accessibility as a function of the puckering angle β . The accessibility is defined as the average S_1-S_0 energy of the given geometry minus the FC bright state energy. The OEEC energy at the geometry with the smallest S_1-S_0 gap is indicated by dashed lines.

Python open-source platform fromage, which we make readily available. This program enables users to easily combine electronic structure codes of their choice for geometry optimization using OEC, OEEC, and SC-OEEC. The current

implementation includes interfaces to popular quantum chemistry programs such as Turbomole, Gaussian, and Molcas. Additional interfaces can be easily implemented, provided that the new codes allow for gradient calculations with point charge embedding.

We have shown that the PCE method is poorly suited to optimizing the geometry of flexible molecules in the crystal form. Consequently, the photochemical conclusions that arise from PCE calculations of such molecules have the potential to be quantitatively and qualitatively erroneous. To overcome this problem, a series of two-level ONIOM(QM:QM') cluster models with Ewald embedding were formulated. They are suitable for geometry optimization of excited state minima and conical intersections.

The potential of these tools was illustrated by applying them to the excited states of two model crystals, HC1 and HC2, displaying excited state intramolecular proton transfer. HC1 displays aggregation induced emission, while HC2 shows no emission in solution or solid state. For both systems, the excitations are clearly localized in one or two molecules, which allowed the emission energies to converge with only a monomer or a dimer in the QM region. We found that using charges originating from molecular or crystal calculations did not significantly impact the results. The emission energy was progressively improved with a hierarchy of embedding models,

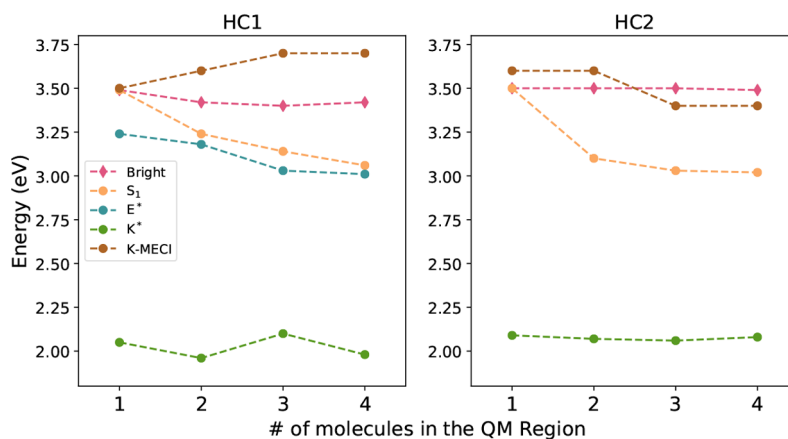


Figure 10. Energy of absorption, emission, and conical intersection as the excited state region increases in size using the OEEC model. The region molecules are added to the region in the order displayed in Figure 4. The energies are evaluated with TD- ω B97X-D/6-31G(d).

ranging from a deviation from the experimental emission peak of 0.8 eV with ONIOM QM:MM to 0.2 eV with OECC. Due to the flexibility of the molecules, this increase in accuracy could only be achieved by carrying out geometry optimization with each embedding model.

Self-consistent procedures help to model the mutual polarization between the excited state region and the environment. In particular, if the self-consistent loop is carried out in the excited state, these procedures may help reflect the delocalization of an excitation despite explicitly modeling fewer excited fragments than are involved in the delocalization. For the systems considered in this study, the degree of localization in both the absorption and emission processes made excited state self-consistent embedding unsuitable. The application of the self-consistent procedure to the ground state did not significantly alter the results obtained from the corresponding non-self-consistent procedure, which suggests that the electronic structure of the isolated ground state molecule is not particularly altered by crystal packing.

With these conclusions in mind, we can suggest optimal embedding methods for the study of the photochemistry of different molecular crystals. If the molecule is certain to be structurally rigid and the exciton couplings are small, the PCE scheme can be appropriate. Otherwise, cluster models are preferred since they allow for exploration of the nuclear configuration space. In either case, long-range electrostatic interactions can account for a significant contribution to the excited state energy. Comparison between excitation energies obtained with truncated cluster models and single point calculations with Ewald embedding methods can help decide whether these methods are required.

The size of the QM region should be motivated by the locality of the excitation at the noteworthy points of the PES which can be estimated by the calculation of exciton couplings between molecular fragments in their lattice positions. These coupling values can, in turn, be estimated as half of the S_2-S_1 energy gap for the dimer⁸¹ or by using more sophisticated methods (see the [Supporting Information](#)). For localized excitations, ground state background charges can be a good choice (either OECC or SC-OECC- S_0). If the excitation is delocalized and the QM region becomes impractically large, the SC-OECC- S_1 method can provide a better description of the excited states. We believe the use of these methods will contribute to a better understanding of complex photochemical processes in the crystal environment, impacting a broad range of applications.

■ ASSOCIATED CONTENT

📄 Supporting Information

The Supporting Information is available free of charge on the ACS Publications website at DOI: [10.1021/acs.jctc.8b01180](https://doi.org/10.1021/acs.jctc.8b01180).

Program specifications for fromage; embedding charges in ONIOM QM:QM'; absorption and emission spectra; population analysis for aggregates; vertical excitation for aggregate; exciton coupling in dimers; results with CC2 and CASPT2 (PDF)

■ AUTHOR INFORMATION

Corresponding Author

*E-mail: r.crespo-otero@qmul.ac.uk

ORCID

Miguel Rivera: 0000-0003-3699-2403

Michael Dommett: 0000-0001-7230-2567

Rachel Crespo-Otero: 0000-0002-8725-5350

Funding

This work was supported by the EPSRC (EP/R029385/1). We acknowledge the support from the School of Biological and Chemical Sciences at Queen Mary University of London.

Notes

The authors declare no competing financial interest.

The fromage code can be found at <https://github.com/Crespo-Otero-group/fromage> and can be contributed to upon request. The modified version of Ewald can be found at <https://github.com/Crespo-Otero-group/Ewald>.

■ ACKNOWLEDGMENTS

This research utilized Queen Mary's Apocrita HPC facility, supported by QMUL Research-IT, ARCHER UK National Supercomputing Service (EP/L000202) via the Materials Chemistry Consortium and the Thomas cluster via our membership to the Thomas Young Centre. The authors thank M. Klintonberg and S. E. Derenzo for allowing the modification and redistribution of the Ewald program and A. A. Sokol for meaningful discussion.

■ REFERENCES

- (1) Li, W.; Pan, Y.; Yao, L.; Liu, H.; Zhang, S.; Wang, C.; Shen, F.; Lu, P.; Yang, B.; Ma, Y. A Hybridized Local and Charge-Transfer Excited State for Highly Efficient Fluorescent OLEDs: Molecular Design, Spectral Character, and Full Exciton Utilization. *Adv. Opt. Mater.* **2014**, *2*, 892–901.
- (2) Jo, S. B.; Kim, H. H.; Lee, H.; Kang, B.; Lee, S.; Sim, M.; Kim, M.; Lee, W. H.; Cho, K. Boosting Photon Harvesting in Organic Solar Cells With Highly Oriented Molecular Crystals via Graphene–Organic Heterointerface. *ACS Nano* **2015**, *9*, 8206–8219.
- (3) Gierschner, J.; Varghese, S.; Park, S. Y. Organic Single Crystal Lasers: A Materials View. *Adv. Opt. Mater.* **2016**, *4*, 348–364.
- (4) Aragón, J.; Troisi, A. Dynamics of the Excitonic Coupling in Organic Crystals. *Phys. Rev. Lett.* **2015**, *114*, 026402.
- (5) Severo Pereira Gomes, A.; Jacob, C. R. Quantum-Chemical Embedding Methods for Treating Local Electronic Excitations in Complex Chemical Systems. *Annu. Rep. Prog. Chem., Sect. C: Phys. Chem.* **2012**, *108*, 222–277.
- (6) Kochman, M. A.; Bil, A.; Morrison, C. A. Hybrid QM/QM Simulations of Photochemical Reactions in the Molecular Crystal N-Salicylidene-2-Chloroaniline. *Phys. Chem. Chem. Phys.* **2013**, *15*, 10803–10806.
- (7) Kochman, M. A.; Morrison, C. A. Hybrid QM/QM Simulations of Excited-State Intramolecular Proton Transfer in the Molecular Crystal 7-(2-Pyridyl)-Indole. *J. Chem. Theory Comput.* **2013**, *9*, 1182–1192.
- (8) Libisch, F.; Huang, C.; Carter, E. A. Embedded Correlated Wavefunction Schemes: Theory and Applications. *Acc. Chem. Res.* **2014**, *47*, 2768–2775.
- (9) Cheng, J.; Yu, K.; Libisch, F.; Dieterich, J. M.; Carter, E. A. Potential Functional Embedding Theory at the Correlated Wave Function Level. 2. Error Sources and Performance Tests. *J. Chem. Theory Comput.* **2017**, *13*, 1081–1093.
- (10) Cheng, J.; Libisch, F.; Yu, K.; Chen, M.; Dieterich, J. M.; Carter, E. A. Potential Functional Embedding Theory at the Correlated Wave Function Level. 1. Mixed Basis Set Embedding. *J. Chem. Theory Comput.* **2017**, *13*, 1067–1080.
- (11) Presti, D.; Labat, F.; Pedone, A.; Frisch, M. J.; Hratchian, H. P.; Ciofini, I.; Menziani, M. C.; Adamo, C. Computational Protocol for Modeling Thermochromic Molecular Crystals: Salicylidene Aniline as a Case Study. *J. Chem. Theory Comput.* **2014**, *10*, 5577–5585.
- (12) Presti, D.; Pedone, A.; Ciofini, I.; Labat, F.; Menziani, M. C.; Adamo, C. Optical Properties of the Dibenzothiazolylphenol Molecular Crystals Through ONIOM Calculations: The Effect of the Electrostatic Embedding Scheme. *Theor. Chem. Acc.* **2016**, *135*, 86.

- (13) Presti, D.; Labat, F.; Pedone, A.; Frisch, M. J.; Hratchian, H. P.; Ciofini, I.; Cristina Menziani, M.; Adamo, C. Modeling Emission Features of Salicylidene Aniline Molecular Crystals: A QM/QM' Approach. *J. Comput. Chem.* **2016**, *37*, 861–870.
- (14) Kantorovich, L. *Quantum Theory of the Solid State: An Introduction*; Springer Netherlands: Dordrecht, 2004.
- (15) Weber, J.; Schmedt auf der Günne, J. Calculation of NMR Parameters in Ionic Solids by an Improved Self-Consistent Embedded Cluster Method. *Phys. Chem. Chem. Phys.* **2010**, *12*, 583–603.
- (16) Torras, J.; Bromley, S.; Bertran, O.; Illas, F. Modelling Organic Molecular Crystals by Hybrid Quantum Mechanical/Molecular Mechanical Embedding. *Chem. Phys. Lett.* **2008**, *457*, 154–158.
- (17) McKenna, K. P.; Sushko, P. V.; Shluger, A. L. Inside Powders: A Theoretical Model of Interfaces Between MgO Nanocrystallites. *J. Am. Chem. Soc.* **2007**, *129*, 8600–8608.
- (18) Kittel, C. *Introduction to Solid State Physics*, 8th ed.; John Wiley & Sons, Inc.: New York, 2005.
- (19) Toukmaji, A. Y.; Board, J. a. Ewald Summation Techniques in Perspective: A Survey. *Comput. Phys. Commun.* **1996**, *95*, 73–92.
- (20) Sauer, J. Molecular Models in Ab Initio Studies of Solids and Surfaces: From Ionic Crystals and Semiconductors to Catalysts. *Chem. Rev.* **1989**, *89*, 199–255.
- (21) Klintonberg, M.; Derenzo, S.; Weber, M. Accurate Crystal Fields for Embedded Cluster Calculations. *Comput. Phys. Commun.* **2000**, *131*, 120–128.
- (22) Derenzo, S. E.; Klintonberg, M. K.; Weber, M. J. Determining Point Charge Arrays That Produce Accurate Ionic Crystal Fields for Atomic Cluster Calculations. *J. Chem. Phys.* **2000**, *112*, 2074–2081.
- (23) Jug, K.; Bredow, T. Models for the Treatment of Crystalline Solids and Surfaces. *J. Comput. Chem.* **2004**, *25*, 1551–1567.
- (24) Stueber, D.; Guenneau, F. N.; Grant, D. M. The Calculation of 13C Chemical Shielding Tensors in Ionic Compounds Utilizing Point Charge Arrays Obtained From Ewald Lattice Sums. *J. Chem. Phys.* **2001**, *114*, 9236–9243.
- (25) Sokol, A. A.; Bromley, S. T.; French, S. A.; Catlow, C. R. A.; Sherwood, P. Hybrid QM/MM Embedding Approach for the Treatment of Localized Surface States in Ionic Materials. *Int. J. Quantum Chem.* **2004**, *99*, 695–712.
- (26) Metz, S.; Kästner, J.; Sokol, A. A.; Keal, T. W.; Sherwood, P. ChemShell-a Modular Software Package for QM/MM Simulations. *Wiley Interdiscip. Rev. Comput. Mol. Sci.* **2014**, *4*, 101–110.
- (27) Abarenkov, I. V. Unit Cell for a Lattice Electrostatic Potential. *Phys. Rev. B: Condens. Matter Mater. Phys.* **2007**, *76*, 165127.
- (28) Sushko, P. V.; Abarenkov, I. V. General Purpose Electrostatic Embedding Potential. *J. Chem. Theory Comput.* **2010**, *6*, 1323–1333.
- (29) Kobayashi, O.; Nanbu, S. Application of Particle-Mesh Ewald Summation to ONIOM Theory. *Chem. Phys.* **2015**, *461*, 47–57.
- (30) Nam, K.; Gao, J.; York, D. M. An Efficient Linear-Scaling Ewald Method for Long-Range Electrostatic Interactions in Combined QM/MM Calculations. *J. Chem. Theory Comput.* **2005**, *1*, 2–13.
- (31) Wang, Y.; Lopata, K.; Chambers, S. A.; Govind, N.; Sushko, P. V. Optical Absorption and Band Gap Reduction in (Fe_{1-x}Cr_x)₂O₃ Solid Solutions: A First-Principles Study. *J. Phys. Chem. C* **2013**, *117*, 25504–25512.
- (32) Sushko, P. V.; Qiao, L.; Bowden, M.; Varga, T.; Exarhos, G. J.; Urban, F. K.; Barton, D.; Chambers, S. A. Multiband Optical Absorption Controlled by Lattice Strain in Thin-Film LaCrO₃. *Phys. Rev. Lett.* **2013**, *110*, 077401.
- (33) Sousa, C.; Tosoni, S.; Illas, F. Theoretical Approaches to Excited-State-Related Phenomena in Oxide Surfaces. *Chem. Rev.* **2013**, *113*, 4456–4495.
- (34) Cui, G.; Yang, W. Conical Intersections in Solution: Formulation, Algorithm, and Implementation With Combined Quantum Mechanics/Molecular Mechanics Method. *J. Chem. Phys.* **2011**, *134*, 204115.
- (35) Wilbraham, L.; Adamo, C.; Labat, F.; Ciofini, I. Electrostatic Embedding to Model the Impact of Environment on Photophysical Properties of Molecular Crystals: A Self-Consistent Charge Adjustment Procedure. *J. Chem. Theory Comput.* **2016**, *12*, 3316–3324.
- (36) Presti, D.; Wilbraham, L.; Targa, C.; Labat, F.; Pedone, A.; Menziani, M. C.; Ciofini, I.; Adamo, C. Understanding Aggregation-Induced Emission in Molecular Crystals: Insights From Theory. *J. Phys. Chem. C* **2017**, *121*, 5747–5752.
- (37) Wilbraham, L.; Louis, M.; Alberga, D.; Brosseau, A.; Guillot, R.; Ito, F.; Labat, F.; Métivier, R.; Allain, C.; Ciofini, I. Revealing the Origins of Mechanically Induced Fluorescence Changes in Organic Molecular Crystals. *Adv. Mater.* **2018**, *30*, 1800817.
- (38) Cieplak, P.; Dupradeau, F.-Y.; Duan, Y.; Wang, J. Polarization Effects in Molecular Mechanical Force Fields. *J. Phys.: Condens. Matter* **2009**, *21*, 333102.
- (39) Warshel, A.; Kato, M.; Pisiakov, A. V. Polarizable Force Fields: History, Test Cases, and Prospects. *J. Chem. Theory Comput.* **2007**, *3*, 2034–2045.
- (40) Xie, W.; Gao, J. Design of a Next Generation Force Field: The X-Pol Potential. *J. Chem. Theory Comput.* **2007**, *3*, 1890–1900.
- (41) Dommett, M.; Crespo-Otero, R. Excited State Proton Transfer in 2'-Hydroxychalcone Derivatives. *Phys. Chem. Chem. Phys.* **2017**, *19*, 2409–2416.
- (42) Dommett, M.; Rivera, M.; Crespo-Otero, R. How Inter- And Intramolecular Processes Dictate Aggregation-Induced Emission in Crystals Undergoing Excited-State Proton Transfer. *J. Phys. Chem. Lett.* **2017**, *8*, 6148–6153.
- (43) Cheng, X.; Wang, K.; Huang, S.; Zhang, H.; Zhang, H.; Wang, Y. Organic Crystals With Near-Infrared Amplified Spontaneous Emissions Based on 2'-Hydroxychalcone Derivatives: Subtle Structure Modification but Great Property Change. *Angew. Chem., Int. Ed.* **2015**, *54*, 8369–8373.
- (44) Crespo-Otero, R.; Li, Q.; Blancafort, L. Exploring Potential Energy Surfaces for Aggregation-Induced Emission - from Solution to Crystal. *Chem. - Asian J.* **2019**, *14*, 700.
- (45) Li, Q.; Blancafort, L. A Conical Intersection Model to Explain Aggregation Induced Emission in Diphenyl Dibenzofulvene. *Chem. Commun.* **2013**, *49*, 5966–5968.
- (46) Rivera, M.; Dommett, M.; Crespo-Otero, R. *fromage: A FRamework for Molecular AGgregate Excitations*; 2018. <https://github.com/Crespo-Otero-group/fromage>.
- (47) Rivera, M.; Dommett, M.; Crespo-Otero, R. Documentation for fromage. 2018. <https://fromage.readthedocs.io/>.
- (48) Frisch, M. J.; Trucks, G. W.; Schlegel, H. B.; Scuseria, G. E.; Robb, M. A.; Cheeseman, J. R.; Scalmani, G.; Barone, V.; Mennucci, B.; Petersson, G. A.; Nakatsuji, H.; Caricato, M.; Li, X.; Hratchian, H. P.; Izmaylov, A. F.; Bloino, J.; Zheng, G.; Sonnenberg, J. L.; Hada, M.; Ehara, M.; Toyota, K.; Fukuda, R.; Hasegawa, J.; Ishida, M.; Nakajima, T.; Honda, Y.; Kitao, O.; Nakai, H.; Vreven, T.; Montgomer, J. A., Jr.; Peralta, J. E.; Ogliaro, F.; Bearpark, M.; Heyd, J. J.; Brothers, E.; Kudin, K. N.; Staroverov, V. N.; Kobayashi, R.; Normand, J.; Raghavachari, K.; Rendell, A.; Burant, J. C.; Iyengar, S. S.; Tomasi, J.; Cossi, M.; Rega, N.; Millam, J. M.; Klene, M.; Knox, J. E.; Cross, J. B.; Bakken, V.; Adamo, C.; Jaramillo, J.; Gomperts, R.; Stratmann, R. E.; Yazyev, O.; Austin, A. J.; Cammi, R.; Pomelli, C.; Ochterski, J. W.; Martin, R. L.; Morokuma, K.; Zakrzewski, V. G.; Voth, G. A.; Salvador, P.; Dannenberg, J. J.; Dapprich, S.; Daniels, A. D.; Farkas, O.; Foresman, J. B.; Ortiz, J. V.; Cioslowski, J.; Fox, D. J. *Gaussian 09*, revision E.01; Gaussian Inc.: Wallingford, CT, 2009.
- (49) Aquilante, F.; Autschbach, J.; Carlson, R. K.; Chibotaru, L. F.; Delcey, M. G.; De Vico, L.; Fdez. Galván, I.; Ferré, N.; Frutos, L. M.; Gagliardi, L.; Garavelli, M.; Giussani, A.; Hoyer, C. E.; Li Manni, G.; Lischka, H.; Ma, D.; Malmqvist, P. Å.; Müller, T.; Nenov, A.; Olivucci, M.; Pedersen, T. B.; Peng, D.; Plasser, F.; Pritchard, B.; Reiher, M.; Rivalta, I.; Schapiro, I.; Segarra-Martí, J.; Stenrup, M.; Truhlar, D. G.; Ungur, L.; Valentini, A.; Vancoillie, S.; Veyrazov, V.; Vysotskiy, V. P.; Weingart, O.; Zapata, F.; Lindh, R. Molcas 8: New Capabilities for Multiconfigurational Quantum Chemical Calculations Across the Periodic Table. *J. Comput. Chem.* **2016**, *37*, 506–541.
- (50) *TURBOMOLE*, version 6.2 2010; A development of University of Karlsruhe and Forschungszentrum Karlsruhe GmbH: 1989–2007; TURBOMOLE GmbH; since 2007. Available from <http://www.turbomole.com>.

- (51) Aradi, B.; Hourahine, B.; Frauenheim, T. DFTB+, a Sparse Matrix-Based Implementation of the DFTB Method. *J. Phys. Chem. A* **2007**, *111*, 5678–5684.
- (52) Levine, B. G.; Coe, J. D.; Martínez, T. J. Optimizing Conical Intersections Without Derivative Coupling Vectors: Application to Multistate Multireference Second-Order Perturbation Theory (MS-CASPT2). *J. Phys. Chem. B* **2008**, *112*, 405–413.
- (53) Ruiz-Barragan, S.; Morokuma, K.; Blancafort, L. Conical Intersection Optimization Using Composed Steps Inside the ONIOM-(QM:MM) Scheme: CASSCF:UFF Implementation with Microiterations. *J. Chem. Theory Comput.* **2015**, *11*, 1585–1594.
- (54) Levine, B. G.; Martínez, T. J. Isomerization Through Conical Intersections. *Annu. Rev. Phys. Chem.* **2007**, *58*, 613–634.
- (55) Barbatti, M.; Ruckebauer, M.; Plasser, F.; Pittner, J.; Granucci, G.; Persico, M.; Lischka, H. Newton-X: A Surface-Hopping Program for Nonadiabatic Molecular Dynamics. *Wiley Interdiscip. Rev. Comput. Mol. Sci.* **2014**, *4*, 26–33.
- (56) Gozem, S.; Melaccio, F.; Valentini, A.; Filatov, M.; Huix-Rotllant, M.; Ferré, N.; Frutos, L. M.; Angeli, C.; Krylov, A. I.; Granovsky, A. A.; Lindh, R.; Olivucci, M. Shape of Multireference, Equation-Of-Motion Coupled-Cluster, and Density Functional Theory Potential Energy Surfaces at a Conical Intersection. *J. Chem. Theory Comput.* **2014**, *10*, 3074–3084.
- (57) Tuna, D.; Lefrançois, D.; Wolański, Ł.; Gozem, S.; Schapiro, I.; Andrúniów, T.; Dreuw, A.; Olivucci, M. Assessment of Approximate Coupled-Cluster and Algebraic-Diagrammatic-Construction Methods for Ground- and Excited-State Reaction Paths and the Conical-Intersection Seam of a Retinal-Chromophore Model. *J. Chem. Theory Comput.* **2015**, *11*, 5758–5781.
- (58) Crespo-Otero, R.; Mardykov, A.; Sanchez-Garcia, E.; Sander, W.; Barbatti, M. Photo-Stability of Peptide-Bond Aggregates: N-Methylformamide Dimers. *Phys. Chem. Chem. Phys.* **2014**, *16*, 18877–18887.
- (59) Barbatti, M.; Crespo-Otero, R. Surface Hopping Dynamics With DFT Excited States. *Top. Curr. Chem.* **2014**, *368*, 415–444.
- (60) Chung, L. W.; Sameera, W. M. C.; Ramozzi, R.; Page, A. J.; Hatanaka, M.; Petrova, G. P.; Harris, T. V.; Li, X.; Ke, Z.; Liu, F.; Li, H. B.; Ding, L.; Morokuma, K. The ONIOM Method and Its Applications. *Chem. Rev.* **2015**, *115*, 5678–5796.
- (61) Presti, D.; Labat, F.; Pedone, A.; Frisch, M. J.; Hratchian, H. P.; Ciofini, I.; Cristina Menziani, M.; Adamo, C. Modeling Emission Features of Salicylidene Aniline Molecular Crystals: A QM/QM' Approach. *J. Comput. Chem.* **2016**, *37*, 861–870.
- (62) Clemente, F. R.; Vreven, T.; Frisch, M. J. *Quantum Biochemistry*; John Wiley & Sons, Ltd.: 2010; Chapter 2, pp 61–83.
- (63) Biancardi, A.; Barnes, J.; Caricato, M. Point charge embedding for ONIOM excited states calculations. *J. Chem. Phys.* **2016**, *145*, 224109.
- (64) Kepenekian, M.; Robert, V.; Le Guennic, B.; De Graaf, C. Energetics of [Fe(NCH)6]2+ via CASPT2 Calculations: A Spin-Crossover Perspective. *J. Comput. Chem.* **2009**, *30*, 2327–2333.
- (65) Le Guennic, B.; Borshch, S.; Robert, V. Prussian Blue Analogue CsFe[Cr(CN)6] as a Matrix for the Fe(II) Spin-Crossover. *Inorg. Chem.* **2007**, *46*, 11106–11111.
- (66) Giannozzi, P.; Baroni, S.; Bonini, N.; Calandra, M.; Car, R.; Cavazzoni, C.; Ceresoli, D.; Chiarotti, G. L.; Cococcioni, M.; Dabo, I.; Dal Corso, A.; de Gironcoli, S.; Fabris, S.; Fratesi, G.; Gebauer, R.; Gerstmann, U.; Gougousis, C.; Kokalj, A.; Lazzeri, M.; Martin-Samos, L.; Marzari, N.; Mauri, F.; Mazzarello, R.; Paolini, S.; Pasquarello, A.; Paulatto, L.; Sbraccia, C.; Scandolo, S.; Sclauzero, G.; Seitsonen, A. P.; Smogunov, A.; Umari, P.; Wentzcovitch, R. M. QUANTUM ESPRESSO: A Modular and Open-Source Software Project for Quantum Simulations of Materials. *J. Phys.: Condens. Matter* **2009**, *21*, 395502.
- (67) Hutter, J.; Iannuzzi, M.; Schiffmann, F.; VandeVondele, J. CP2K: Atomistic Simulations of Condensed Matter Systems. *Wiley Interdiscip. Rev. Comput. Mol. Sci.* **2014**, *4*, 15–25.
- (68) Henkelman, G.; Arnaldsson, A.; Jónsson, H. A Fast and Robust Algorithm for Bader Decomposition of Charge Density. *Comput. Mater. Sci.* **2006**, *36*, 354–360.
- (69) Sanville, E.; Kenny, S. D.; Smith, R.; Henkelman, G. Improved Grid-Based Algorithm for Bader Charge Allocation. *J. Comput. Chem.* **2007**, *28*, 899–908.
- (70) Yu, M.; Trinkle, D. R. Accurate and Efficient Algorithm for Bader Charge Integration. *J. Chem. Phys.* **2011**, *134*, 064111.
- (71) Tang, W.; Sanville, E.; Henkelman, G. A Grid-Based Bader Analysis Algorithm Without Lattice Bias. *J. Phys.: Condens. Matter* **2009**, *21*, 084204.
- (72) Zahid, N. I.; Mahmood, M. S.; Subramanian, B.; Mohd Said, S.; Abou-Zied, O. K. New Insight Into the Origin of the Red/Near-Infrared Intense Fluorescence of a Crystalline 2-Hydroxychalcone Derivative: A Comprehensive Picture From the Excited-State Femtosecond Dynamics. *J. Phys. Chem. Lett.* **2017**, *8*, 5603–5608.
- (73) Crespo-Otero, R.; Barbatti, M. Spectrum Simulation and Decomposition With Nuclear Ensemble: Formal Derivation and Application to Benzene, Furan and 2-Phenylfuran. *Theor. Chem. Acc.* **2012**, *131*, 1237.
- (74) Barbatti, M.; Granucci, G.; Ruckebauer, M.; Plasser, F.; Crespo-Otero, R.; Pittner, J.; Persico, M.; Lischka, H. NEWTON-X: A Package for Newtonian Dynamics Close to the Crossing Seam, version 2; 2016. www.newtonx.org.
- (75) Wilbraham, L.; Savarese, M.; Rega, N.; Adamo, C.; Ciofini, I. Describing Excited State Intramolecular Proton Transfer in Dual Emissive Systems: A Density Functional Theory Based Analysis. *J. Phys. Chem. B* **2015**, *119*, 2459–2466.
- (76) Presti, D.; Wilbraham, L.; Targa, C.; Labat, F.; Pedone, A.; Menziani, M. C.; Ciofini, I.; Adamo, C. Understanding Aggregation-Induced Emission in Molecular Crystals: Insights From Theory. *J. Phys. Chem. C* **2017**, *121*, 5747–5752.
- (77) Skelton, J. M.; Lora da Silva, E.; Crespo-Otero, R.; Hatcher, L. E.; Raithby, P. R.; Parker, S. C.; Walsh, A. Electronic Excitations in Molecular Solids: Bridging Theory and Experiment. *Faraday Discuss.* **2015**, *177*, 181–202.
- (78) Peng, X.-L.; Ruiz-Barragan, S.; Li, Z.-S.; Li, Q.-S.; Blancafort, L. Restricted Access to a Conical Intersection to Explain Aggregation Induced Emission in Dimethyl Tetraphenylsilole. *J. Mater. Chem. C* **2016**, *4*, 2802–2810.
- (79) Crespo-Otero, R.; Barbatti, M. Recent Advances and Perspectives on Nonadiabatic Mixed Quantum–Classical Dynamics. *Chem. Rev.* **2018**, *118*, 7026–7068.
- (80) Barbatti, M.; Lan, Z.; Crespo-Otero, R.; Szymczak, J. J.; Lischka, H.; Thiel, W. Critical Appraisal of Excited State Nonadiabatic Dynamics Simulations of 9H-Adenine. *J. Chem. Phys.* **2012**, *137*, 22A503.
- (81) Spano, F. C.; Beljonne, D. In *The WSPC Reference on Organic Electronics: Organic Semiconductors*; Bredas, J.-L., Marder, S. R., Eds.; World Scientific: Hackensack, NJ, 2016; Chapter 4, pp 93–130.